Detecting Protein Complexes in Living Cells from Laser Scanning Confocal Image Sequences by the Cross Correlation Raster Image Spectroscopy Method

Michelle A. Digman,[†] Paul W. Wiseman,[‡] Alan R. Horwitz,[§] and Enrico Gratton[†*]

[†]Laboratory for Fluorescence Dynamics and Department of Biomedical Engineering, University of California, Irvine, California; [‡]Departments of Chemistry and Physics, McGill University, Montreal, Quebec, Canada; and [§]Department of Cell Biology, School of Medicine, University of Virginia, Charlottesville, Virginia

ABSTRACT We describe a general method for detecting molecular complexes based on the analysis of single molecule fluorescence fluctuations from laser scanning confocal images. The method detects and quantifies complexes of two different fluorescent proteins noninvasively in living cells. Because in a raster scanned image successive pixels are measured at different times, the spatial correlation of the image contains information about dynamic processes occurring over a large time range, from the microseconds to seconds. The correlation of intensity fluctuations measured simultaneously in two channels detects protein complexes that carry two molecules of different colors. This information is obtained from the entire image. A map of the spatial distribution of protein complexes in the cell and their diffusion and/or binding properties can be constructed. Using this cross correlation raster image spectroscopy method, specific locations in the cell can be visualized where dynamics of binding and unbinding of fluorescent protein complexes occur. This fluctuation imaging method can be applied to commercial laser scanning microscopes thereby making it accessible to a large community of scientists.

INTRODUCTION

The past two decades have produced a revolution in optical microscopy. Nonlinear excitation, stimulated emission, and more recently, single molecule imaging, for example, have pushed the limits of optical resolution to new frontiers (1–4). Despite these advances, however, a need remains for a robust method for detecting protein complexes in living cells. Because cellular processes are often localized and transient, the ideal method would have high spatial resolution, and the data should be acquired within the timescale of the biological process under investigation.

Generally, the existence of molecular complexes is inferred biochemically using coimmunoprecipitation and then confirmed by fluorescence colocalization or FRET (5,6). Colocalization, even at the super resolution achievable with the most recent fluorescence methods, does not show that the molecules of interest actually reside in a structural complex. Whereas molecules residing within ~5 nm show FRET under ideal situations, two different molecules within a structurally defined complex, which contains several different molecular species, may not be close enough for FRET. Furthermore, molecules that do not reside in the same structural complex but are near each other can exhibit FRET.

Fluorescence correlation spectroscopy, which is based on dynamic colocalization, is an alternative approach (7). However, fluorescence cross correlation methods are based traditionally on the measurement of temporal fluctuations at a single point in the cell. In this mode, measuring cross correlated fluctuations at a single point is difficult to interpret in living cells because of possible correlations due to movement of macroscopic objects. In addition, it requires that the observer choose a point of interest before the measurement begins. Thus, a method is desired that can separate the obvious correlations due to the movements of macroscopic objects and at the same time provide a map of the location of specific molecular complexes.

Confocal fluorescence microscopy has revolutionized the biomedical field and allowed monitoring of biological processes in live cells in 3D and in real time. However, the wealth of information contained in the confocal image has not been fully exploited to date. We show that we can determine molecular interactions directly in live cells from confocal images. In general, intensity fluctuations are caused by diffusion or binding/unbinding interactions of the protein complex. The coincidence of fluctuations occurring at two detection channels shows that the two proteins are part of the same complex.

In this study, we exploit the raster-scan image correlation spectroscopy (RICS) method that can analyze the diffusion and binding dynamics of molecules in an entire, single image rather than at single points on an image (8,9). We extend the RICS approach to extract the spatial and temporal information provided by the cross correlation between two different types of proteins measured using two detection channels. The basis of the RICS method has been described previously (8). Briefly, in a raster scanned image, the fluorescence intensity of different pixels are measured in a temporal sequence. If molecules move on the timescale of the scan speed, which is microseconds along each scan line and milliseconds between lines, the spatial correlation function for the image

Submitted August 7, 2008, and accepted for publication September 22, 2008.

*Correspondence: egratton22@yahoo.com

Editor: Alberto Diaspro.

0006-3495/09/01/0707/10 $2.00

doi: 10.1016/j.bpj.2008.09.051

is affected by the movement of molecules from a previously scanned pixel to the new pixel being scanned. When done on each image of an image series, we can extract the time information associated with diffusion processes and binding-unbinding equilibria in different parts of an image over a time window that includes most biological processes. The RICS approach can be extended to pairs of molecules, using two-color cross correlation, to measure the diffusion of protein complexes, estimate the fraction of interacting molecules, and determine the temporal and spatial distribution of these complexes. This method, which we call cross correlation RICS (ccRICS), is generally applicable and can be done using commercial, one photon, scanning confocal laser microscopes (10). ccRICS differs in concept from other image based correlation measurements, e.g., image cross correlation spectroscopy (ICCS) (11). The later, for example, correlates intensity fluctuations of pixels or pixel regions among images in a sequence rather than that of the pixels along the raster scan of a single image. Because of this difference, ICCS and other imaged based methods are limited to changes on the timescale of seconds, whereas ccRICS widens the time regime to processes as fast as cytoplasmic diffusion (12).

In this study, we apply ccRICS to a set of adhesions molecules that are known to associate in solution by coimmunoprecipitation. We show that we can distinguish between cytoplasmic diffusion and binding and generate maps of molecular interactions and the dynamics of these interactions across the cell. We also show that these molecules do not reside in complexes when they are diffusing in the cytoplasm but do reside in complexes in the vicinity of disassembling adhesions. These molecules in these complexes show no FRET indicating that in the complex the proteins are at a distance at which FRET is not taking place. From these observations, a model emerges in which adhesions assemble along a scaffold that serves to increase the effective concentration and thereby promote binding interactions, and they disassemble by releasing complexes that rapidly disassociate.

These studies show the rich content of the ccRICS analysis. Interaction maps can be drawn among rapidly diffusing complexes (in the μs-ms timescale), complexes undergoing binding and unbinding interactions (in the ms to s timescale) and changes in the spatial distribution of complexes in response to stimulation that occurs in minutes. The method is noninvasive, and the same cell can be observed for long periods. The map of protein interactions and the dynamics of the interactions cannot be obtained using the co-immuno precipitation methods, and FRET is of only limited use in studying complexes that contain many molecules.

The ccRICS approach

In the ccRICS experiment, data are acquired in two channels simultaneously. The two channels can contain data from two spectral band passes or two polarization directions. When two channels are acquired simultaneously in the confocal microscope, they need to overlap well without significant spectral bleed through as discussed in the Methods section.

In the RICS analysis, we calculate the 2D spatial correlation function (8). The mathematical operation consists of multiplying the matrix corresponding to the image by itself at different shifts in the x and y directions. For ccRICS the two images to be multiplied come from the two channels. Note that the ccRICS is nonsymmetric with respect to the order of the channels:

$$G_{\mathrm{ccRICS}}(\xi,\psi) = \frac{\langle I_1(x,y)I_2(x+\xi,y+\psi)\rangle}{\langle I_1(x,y)\rangle\langle I_2(x,y)\rangle} - 1. \quad (1)$$

The variables ξ and ψ represent spatial increments in the x and y directions, respectively. The 2D spatial correlation is computed more efficiently using FFT methods rather than by the formula above (13).

Whereas the RICS correlation function is sensitive only to fluctuations of the signals in the individual channel, the ccRICS is different from zero only when the intensity fluctuations of the signals in the two detection channels are correlated. Of course, there is always bleed through of one channel into another (generally the *green* into the *red*). In the absence of other correlations, bleed through will give 100% correlation between the two channels.

The amplitude of the correlation at shift (0,0) shows the magnitude of the autocorrelation and of the cross correlation. For two uncorrelated species, the amplitude of the cross correlation at shift 0,0 is proportional to:

$$G_{\mathrm{ccRICS}}(0,0) \propto \left[\frac{f_{11}f_{12}\langle N_1\rangle + f_{21}f_{22}\langle N_2\rangle}{f_{11}f_{12}\langle N_1\rangle^2 + (f_{11}f_{22}+f_{21}f_{12})\langle N_1\rangle\langle N_2\rangle + f_{21}f_{22}\langle N_2\rangle^2}\right], \quad (2)$$

where $\langle N_1\rangle$ and $\langle N_2\rangle$ are the average number of molecules of species 1 and 2 in the volume of excitation. f_{11}, f_{12}, (f_{21} and f_{22}) are the fractional fluorescence intensities of species 1 (species 2) as seen by channel 1 and by channel 2, respectively. f_{12}, f_{21}, represent the bleed through of channel 1 into 2 and vice versa.

The range of the cross correlation signal achievable is restricted to be equal, at most, to the amplitude of the autocorrelation ($G_{cc}(0,0) <= G_{1\ or\ 2}(0,0)$). The minimum value is more difficult to predict because in principle the amplitude could be negative if there is anti correlation, which could occur if there are dynamic processes in the protein complex itself. For ''static'' protein complexes, the minimum value of the amplitude of the cross correlation is given by the amount of bleed through and by the amount of uncorrelated signal. The uncorrelated fluctuation, which arises either from background fluorescence or from molecules that are uncorrelated, has the effect of strongly reducing the correlation due to bleed through.

METHODS

Cell culture and protein transfection

Mouse embryonic fibroblasts (MEF) were grown at 37°C in a 5% CO_2 humidified incubator. The cells were trypsinized, subcultered and transferred from a 35-mm tissue culture flask to a 25 mm, 6-well Falcon tissue culture (Becton-Dickinson, Bedford, MA). They were grown to 50–80% confluence and transfected with 1 μg of DNA (0.5 μg of DNA/protein for cotransfections) and 5 μg of Lipofectamine 2000 obtained from Invitrogen (Carlsbad, CA). Vinculin, focal adhesion kinase (FAK), and paxillin cDNA were ligated to EGFP or mCherry at the C-terminal end. The FAK mutant, I937E/I999E was ligated to EGFP at the C-terminal end. After 24 h of transfection cells were trypsinized and plated using high glucose DMEM media (Pierce-Hyclone, Logan, UT) supplemented with 10% FBS and PEN/STREP on MatTek (Ashland, MA) imaging dishes coated with 3 μg of fibronectin from Sigma-Aldrich (St. Louis, MO) 1 h before imaging.

Microscopy

We used an Olympus FV1000 microscope with a 60× 1.2NA water objective (Olympus, Tokyo, Japan). The scan speed was set at 12.5 μs/pixel. The scan area was 256 × 256 pixels and ~100 to 200 frames were collected for each sample. The corresponding line time was 4.325 ms and the frame time was 1.15 s. The electronic zoom of the microscope was set to 16.3, which corresponds to a region of 12.5 μm^2. For the EGFP excitation, we used the 488 nm line of the argon ion laser and for the mCherry excitation we used 559 nm excitation. The power of the 488 nm laser was set at 0.5% according to the power slider in the FV1000 microscope. When the slider is set to 100%, the power at the sample was 0.7 mW; we verified that the slider operated linearly in the range used. For the red laser, when the slider was set to 100%, the power was 0.1 mW at the sample. The power of the red laser was then changed to match the average intensity in the two channels. Generally, the power in the red channel was <1.5%. Data were collected in the pseudo photon counting mode of the Olympus FV1000 microscope. The filters for the green and red emission channels have a nominal bandwidth of 505–540 nm and 575–675 nm, respectively. The overlap of the volume of observation and excitation at the two colors of our experiments was tested by imaging single 100 nm fluorescent beads carrying two colors simultaneously (yellow-green fluorospheres; Invitrogen). We imaged single immobilized beads using a z-stack with images acquired every 500 nm in the z direction. We found that in the FV1000 microscope the center of mass of the excitation volumes were coincident within 20 nm in the x and y direction and within ~40 nm in the z direction in both channels.

ccRICS analysis

We used the SimFCS program (Laboratory for Fluorescence Dynamics) for RICS and ccRICS analyses. For the RICS analysis data were collected in the 256 × 256 frame format. Fitting of the RICS functions was carried out according to the equations for diffusion as described in Digman et al. (8) and are presented below. The $G(0,0)$ term, which contains the shot noise, is omitted from the analysis. One of the features of the RICS analysis is that slowly varying signals (fluctuations) can be removed from the calculation using a high-pass filter operation implemented by a moving average operation (8). The moving average processing of the image stack removes the spatial correlations due to the immobile fraction and the correlations due to slowly moving features in an image. The length of the moving average determines the timescale of processes that are filtered out by this mathematical procedure. For the calculation of the scan analysis, a small region of interest (64 × 64 pixels) was systematically moved across the image by steps of 32 pixels providing a partial superposition of the regions explored.

Subtraction of the immobile fraction

The RICS analysis consists of calculating the image spatial correlations. This also contains the intensity correlations due to the image features. Because we are only interested in the fluctuating part of the signal, the average image is subtracted before calculating the spatial correlations. To obtain the average image we collect several (~100–200) frames from the image stack. The average of these frames produces the average image, which is then subtracted, pixel-by-pixel, from each of the images of the stack. After subtraction, the average difference has a value close to zero. To avoid dividing by zero, when calculating the spatial correlation function, and to properly normalize the RICS function after subtraction of the immobile fraction, we add a number equal to the average of the average image to each pixel of the subtracted images. If the image features vary slowly, due to cell movement for example, we perform the subtraction operation using only few frames of the stack chosen symmetrically around the image of the stack that will be subtracted. The number of frames included in the local average is determined by the moving average length parameter. If the moving average length is small, i.e., only a few frames, slow variations from frame to frame are effectively removed. By changing the length of the moving average, we can specify the timescale of slow intensity fluctuations that will be included in the fluctuation analysis. For example, using a moving average of 10 (MAV10) all the fluctuations longer than 10 frames (10 s in our case) are removed. Using a moving average of 40 (MAV40) only the very long fluctuations lasting 40 s or more are removed. Note that this operation only affects the slow fluctuations that propagate from frame to frame. The fast fluctuations that only propagate from pixel to pixel or from line to line are not affected by the moving average subtraction algorithm.

Macroscopic correlations

In the RICS approach, we calculate only the spatial correlations in one frame. Bleaching or other intensity changes that propagate from frame to frame do not affect, in principle, the RICS calculation. However, because the frame-to-frame information is used to subtract the immobile (or quasi-immobile) features of the image, the immobile subtraction algorithm will not remove sudden changes in shape or position. These macroscopic changes should not be confused with the correlation in position and intensity due to point particles. Most of the methods based on fluctuations and using camera acquisition are sensitive the changes of pixel intensity from frame to frame. As such, these techniques are substantially different from the RICS approach. In fact, the fast diffusive motion of small molecular aggregates is averaged out due to the long exposure time of the camera and the pixel to pixel correlation (in the same frame) cannot be used because each pixel of the frame is acquired at the same time.

Binding-unbinding equilibria

If one point in the image suddenly changes intensity due to bleaching, binding, or blinking, these changes contribute to the RICS signal because from pixel to pixel or from line to line the intensity fluctuation correlates to neighboring pixels within the size of the point spread function. However, if the immobile fraction removal algorithm is carried out with a very short moving average length, the spatial effect of the local change in intensity rapidly disappears from the image stack. For slow equilibria, the amplitude of the correlation tends to decrease as the moving average length decreases. Instead, if the binding-unbinding process is fast, the subtraction algorithm will not influence the amplitude of the correlation. Fig. 1 shows simulations of diffusion and binding–unbinding equilibria with different rates and the effect on the RICS function. Fast diffusion always gives an elongated shape along the x (fast) axis in the RICS function due to the probability to correlate the same particle at a distance whereas slow binding equilibria give a round shape because the process occurs at specific locations (Fig. 1, *left column*). In the central column of Fig. 1 we simulated particles binding in rapid (in the ms timescale) equilibria to fixed locations. Because the dynamics occurs in times comparable to the line time, when the position of the particle is visited again at the next line, the intensity at this location appears to blink rapidly. In the third column we simulated binding events occurring at a much slower timescale, comparable to the frame time. In all cases, the shape of the

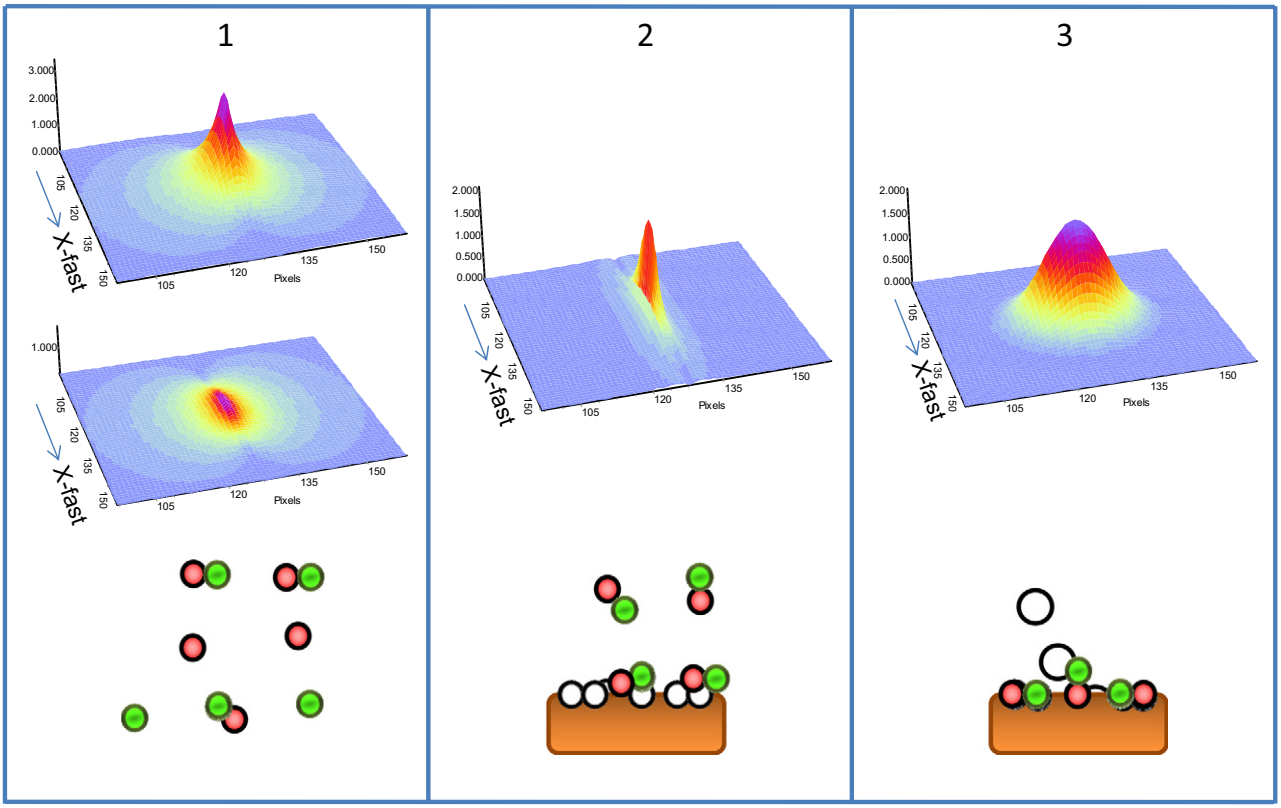

FIGURE 1 Simulation of particles diffusing and binding to fixed locations. Column 1: simulation of 100 particles of two different colors diffusing in a square surface with a diffusion constant of 5 $\mu m^2/s$. Ten particles, carrying both colors are diffusing in the same area with the same diffusion constant. The upper panel shows the RICS function obtained from analyzing the data at one channel and the second panel shows the ccRICS. The intensity of the green particles bleeds into the red channel (2%) to simulate bleed through. Under this condition, in which there are red particles diffusing, the bleed through causes a very small difference on the amplitude of the ccRICS. Column 2: particles bind and unbind rapidly (with respect to the line time) to and from fixed locations. The RICS (autocorrelation) or ccRICS have the same shape. This shape is quite different from the shape obtained with particles diffusing. In the x direction, the shape is related to the extension of the illumination volume. Column 3: particles undergo slow (with respect to the line time) binding equilibria. The shape of the RICS (or ccRICS) is related to the shape of the illumination volume.

RICS function is substantially different for these two processes: diffusion and binding. Only when the binding (or blinking) is extremely fast (in the microsecond timescale), the RICS function due to fast diffusion and blinking of immobile molecules tends to have similar shape, however, most biological binding equilibria are not that fast.

Bleed through artifacts

The molecular information from the ccRICS can be compromised if there is a large bleed through between the two channels. We measured the bleed through in our microscope and filter combination using cells expressing only one color; it was ~2% of the green emission into the red channel. The bleed through of the red emission into the green channel was below 1%. As we discussed in the manuscript, the cross correlation amplitude can be at most as large as the autocorrelation. A way to express the amount of cross correlation is to normalize the amplitude of the cross correlation to the amplitude of the autocorrelation, resulting in an index of cross correlation between 0 and 1. The question is how can we distinguish true cross correlation from bleed through?

According to the expression for the $G(0,0)$ in Eq. 2, the index of the ccRICS signal will be 1 due to bleed through if only one species is present in the sample. Therefore, to properly interpret the cross correlation index, we need to estimate the spectral bleed through and the amount of signal in the two channels. In our cellular systems, we have some autofluorescence, which is less 10% of the total fluorescence and approximately an equal number of green and red molecules. If all molecules will be uncorrelated, the presence of bleed through (2%) will give a cross correlation index of 0.04 according to Eq. 2. This estimation will be incorrect if we had much less red molecules than green molecules. In Table 1 we report several measurements with a cross correlation index below 0.1 and in some cases below 0.05. When the index is below 0.05, we attribute this value to bleed through. In general, it seems that the bleed through between the two channels does not impact our conclusions about the existence and quantification of protein complexes because in many cases we observe cross correlation indexes well above 0.05. Because the bleed through is small in our instrument, the value of the cross correlation index (from 0 to 1) is approximately equal to the fraction of correlated molecules so that the value of this index can be directly related to the fraction of complexes containing both molecules. Accordingly, we should be able to observe even 5% of molecules carrying both colors.

Equations used for fitting the RICS function

The RICS correlation function in its simpler form can be written as the product of two terms. One term corresponds to the effect of diffusion and how the intensity at one pixel propagates to the next neighbor pixel. This term is similar to the normal time dependent term in fluctuation spectroscopy but it accounts for the difference in time between the horizontal line and the vertical line in the raster scan data acquisition method:

TABLE 1

	G_1	D_1 (μm^2/s)	G_2	D_2 (μm^2/s)	G_{cc}	D_{cc} (μm^2/s)	$G_{cc}/Av(G_1,G_2)$
VIN-PAX moving average of 10							
Cell 1	0.0045	12.4	0.0078	5.7	0.0005	1.2	0.08
Cell 2(*)	0.0061	13.0	0.016	8.1	0.0001	0.9	0.01
Cell 3(*)	0.0069	11.1	0.0082	6.1	0.0001	1.0	0.01
Cell 4	0.0031	8.6	0.0041	8.2	0.0006	2.1	0.18
VIN-PAX moving average of 40							
Cell 1	0.0078	2.4	0.0116	2.0	0.0034	0.8	0.35
Cell 2(*)	0.0071	6.5	0.021	4.8	0.0003	0.8	0.02
Cell 3(*)	0.0082	8.0	0.0115	3.9	0.0004	1.3	0.04
Cell 4	0.0041	5.2	0.0052	4.8	0.0014	1.5	0.30
FAK-PAX moving average of 10							
Cell 1	0.0046	4.4	0.0050	7.1	0.0006	0.8	0.12
Cell 2	0.010	4.3	0.0095	6.4	0.0004	0.7	0.04
Cell 3	0.020	5.1	0.021	5.4	0.0037	1.44	0.18
FAK-PAX moving average of 40							
Cell 1	0.0065	2.3	0.0068	3.5	0.0024	1.0	0.36
Cell 2	0.0122	3.2	0.0115	3.7	0.0017	0.5	0.14
Cell 3	0.0327	3.2	0.0379	3.1	0.014	0.8	0.36

G is the $G(0,0)$ term and D is the apparent diffusion coefficient. Indexes 1, 2, and cc refer to channel 1, channel 2, and the cross correlation between the two channels, respectively.
*Indicates quiescent regions of the cell.

$$G_D(\xi,\psi) = \frac{\gamma}{N}\left(1 + \frac{4D(\tau_p\xi + \tau_l\psi)}{w_0^2}\right)^{-1} \times \left(1 + \frac{4D(\tau_p\xi + \tau_l\psi)}{w_z^2}\right)^{-1/2}. \quad (3)$$

In this equation, D is the diffusion coefficient in units of μm^2/s, τ_p and τ_l are the pixel dwell time and the line time in s, respectively and w_0 is the waist ($1/e^2$) of the PSF in microns. γ is a factor that account for the profile of illumination (0.35 for 3D Gaussian and 0.076 for Gaussian Lorentzian, respectively) and N is the number of molecules in the excitation volume. The second term of the RICS autocorrelation function reflects the apparent broadening of the PSF due to the diffusion of molecules. In the absence of diffusion, this term is just the spatial correlation of the PSF, which we describe with a Gaussian. When diffusion is present, the width of this Gaussian term becomes time dependent as shown below:

$$S(\xi,\psi) = \exp\left(-\frac{\left(\frac{\delta r}{w_0}\right)^2(\xi^2 + \psi^2)}{\left(1 + \frac{4D(\tau_p\xi + \tau_l\psi)}{w_0^2}\right)}\right). \quad (4)$$

In this expression, δr is the pixel size, in microns.

The overall RICS correlation function is given by the product of the two terms above:

$$G(\xi,\psi) = G_D(\xi,\psi) \cdot S(\xi,\psi). \quad (5)$$

RESULTS

Fig. 2 shows the images of a mouse embryo fibroblast, expressing vinculin-EGF (*green channel*) and paxillin-mCherry (*red channel*) whose fluorescence is captured in the two different channels. These two proteins colocalize well as shown by comparing the images in the two channels and their RGB overlay (Fig. 2, *A–C*). FAK-EGFP and paxillin-mCherry colocalize similarly (Fig. 3). However, we were unable to observe FRET using either intensity methods or FLIM (data not shown). Thus despite the colocalization and their coimmunopurification, there is no direct evidence suggesting that they interact in cells. In the Supporting Material, we show movies of the image stacks used for Figs. 2 and 3 for the green and red channels, respectively. These movies show the apparent movement of the adhesions.

In contrast, both pairs (vinculin-EGFP and paxillin-mCherry and FAK-EGFP and paxillin-mCherry) cross-correlated, which shows that they interact in cells. Figs. 2 and 3 show the RICS autocorrelation and cross correlation functions for vinculin-paxillin and FAK-paxillin, respectively. We used two different moving average lengths for the removal of the immobile fraction. The first row of RICS functions (Figs. 2 and 3, *D–F*) were obtained with a high pass filter (moving average of 10 frames) that corresponds to ~11.5 s; i.e., all processes from microseconds to ~11.5 s are present in the RICS function. The presence of RICS autocorrelation for each of the individual channels shows that both vinculin and paxillin are diffusing relatively rapidly in the cytoplasm. The characteristic elongated shape of the RICS function along the fast scan axis (Figs. 2 and 3) shows that the molecules are moving fast relative to the line scanning time, which is ~4.325 ms. Table 1 reports the results from fitting the RICS function using a one-species diffusion model (8) for several cells.

The amplitude of the ccRICS function (Fig. 2 *F*), using the 10-frame moving average, is much less than that for the autocorrelation (Fig. 2 *D*). This small ccRICS signal likely corresponds to a small amount of spectral bleed through. However, when the moving average is set to 40 frames (Fig. 2 *I*), the amplitude of the ccRICS increases

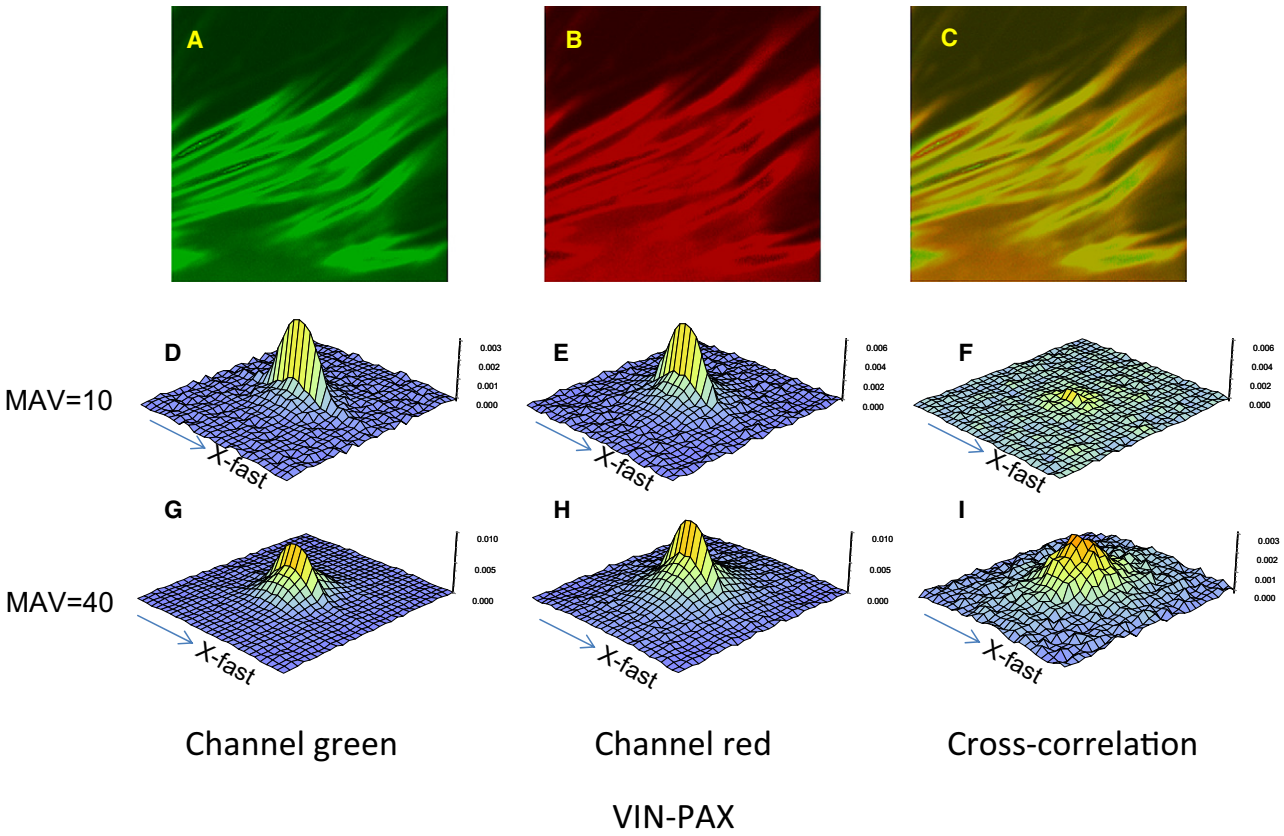

FIGURE 2 (*A–C*) Intensity images of a cell expressing vinculin-EGFP and paxillin-mCherry in the green and red channels and the RGB composition of the green and red channels. The size of the image is 12.5 μm by 12.5 μm. (*D–F*) RICS auto (channel 1 and 2) and cross correlation (ccRICS) signal using a moving average of 10 frames to remove the quasi-immobile components. The RICS function is the representation of the autocorrelation function described by Eq. 1 (see text). The axes in the plane represents the ξ and ψ increments and the vertical axis is the $G(\xi,\psi)$ function. (*G–I*) RICS functions obtained using a moving average of 40 frames. The fits of the RICS data using one diffusion component are shown in Table 1.

substantially showing molecular interaction. In Table 1 we report the ratios between the G(0) obtained for the ccRICS and the G(0) obtained for the average RICS signal (autocorrelation) in the two channels. This ratio is relatively small (<0.1) when the moving average length is set at 10 frames but increases to ~0.4 when the moving average length is set to 40 frames (Fig. 2 *I*). For the data analyzed with the moving average of 40, the shape of the ccRICS function is round, rather than elongated, and it has the size of the point spread function (PSF). This shows that the correlated movements of the two proteins at this (slower) timescale are due to localized binding-unbinding equilibria rather than diffusion. If we use the entire stack to calculate the average image intensity, the overall macroscopic apparent motion of the entire adhesion starts to show in the shape of the RICS function.

The ccRICS analysis was repeated for the pair FAK-EGFP and paxillin-mCherry (Fig. 3). Again, we found individual molecules diffusing rapidly in the cytoplasm but there was no cross correlation using a moving average of 10 frames (Fig. 3 *F*). This shows that the two molecular species are diffusing rapidly, but independently. However, when we increased the length of the moving average operation to emphasize slower fluctuations, the ccRICS signal became significant (Fig. 3 *I*). The shape of the RICS function for the slow process was no longer elongated and approximated the size of the point spread function, showing that the cross correlated events correspond to slow binding-unbinding equilibria, as described above. Interestingly, the ratio of the amplitudes of the ccRICS to the RICS autocorrelation functions for this pair in this particular cell is smaller than that for the vinculin-paxillin pair.

Although the above analyses were obtained by averaging the spatial correlations over the entire frame, the RICS analysis also can show interactions in a smaller region(s) of interest (ROI), thus providing a map of where the protein interactions occur within the cell. To show any local differences in the interactions, we systematically calculated the ccRICS in a small ROI (64 $\times$ 64 pixels) scanned across the entire image. We normalized the ccRICS by dividing the $G(0,0)$ of the cross correlation signal by the average of the autocorrelation function for the two channels in the same ROI. We found that the ccRICS signal is higher in the regions where the focal adhesions are disassembling, e.g., at the upper and right border of the image in Fig. 4 *A*.

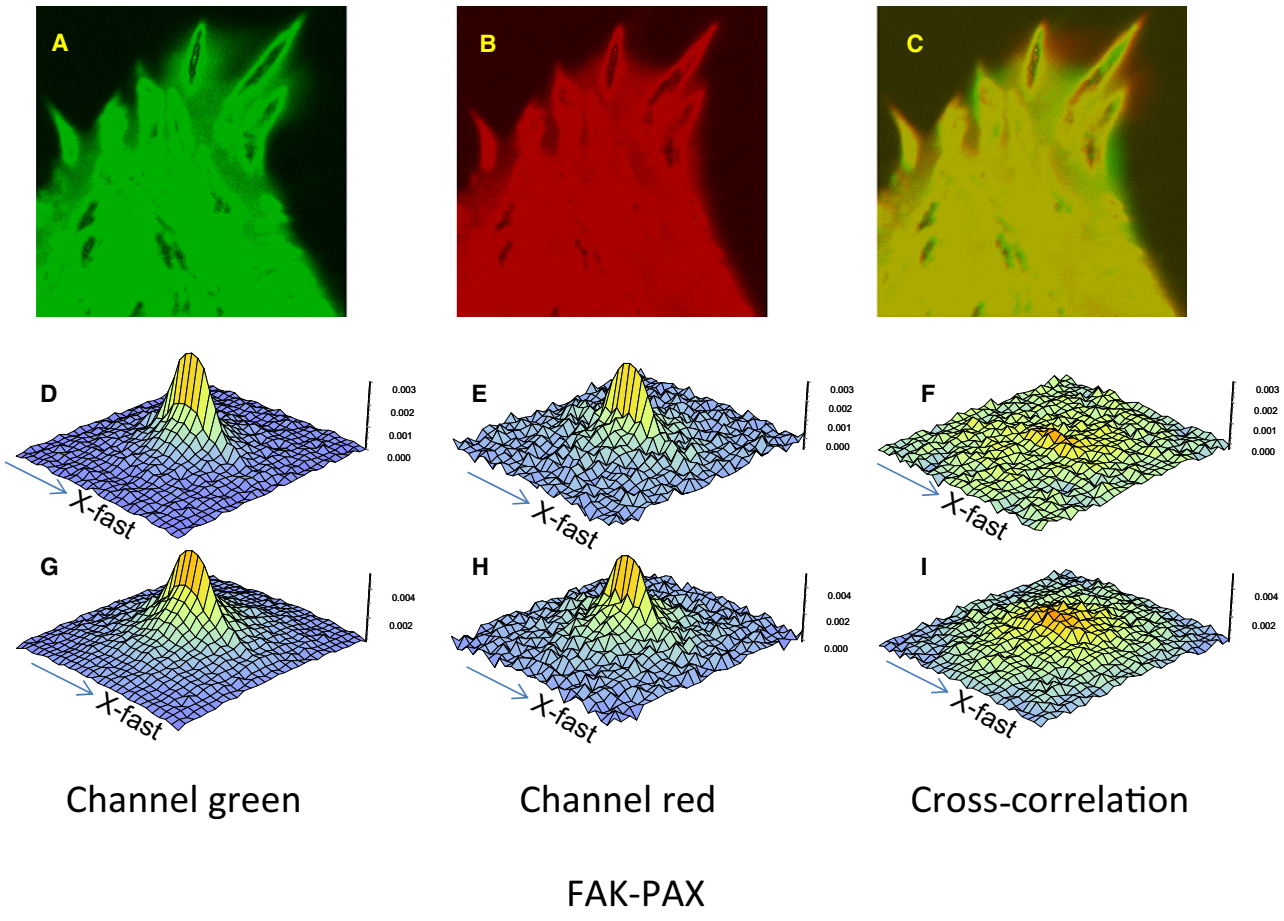

FIGURE 3 (*A–C*) Intensity images of a cell expressing FAK-EGFP and paxillin-mCherry in the green and red channels and the RGB composition of the green and red channels. The size of the image is 12.5 μm by 12.5 μm. (*D–F*) RICS auto (channel 1 and 2) and cross correlation signal using a moving average of 10 frames to remove the quasi-immobile components. (*G–I*) RICS functions obtained using a moving average of 40 frames. The fits of the RICS data using one diffusion component are shown in Table 1.

We interpreted this cross correlation as due to complexes containing both proteins that are being released from adhesions during their disassembly. Little or no cross correlation is seen away from disassembling adhesions, suggesting that the complexes, after detaching from the adhesions, have only a brief life, and fall apart quickly. It also suggests that there are few if any preassembled complexes in the general cytoplasm or associated with the other adhesions, on this timescale. Fig. 4 *B* uses a moving average of 40 frames. This analysis emphasizes the locations in the cell where binding equilibria are more prominent. The map of these interactions has large amplitude in the upper-right part of the image, where adhesions are disassembling and ''sliding'' toward the lower left corner of the image. This suggests that complexes containing both molecules release from adhesions that are disassembling and/or sliding.

Cross correlation of a mutant of FAK that does not bind to Paxillin

As a control we present the RICS and ccRICS analysis of a cell expressing a FAK mutant that is not supposed to bind to paxillin (Fig. 5). For this cell, the FAK mutant labeled with EGFP does not concentrate at the adhesions whereas paxillin-mCherry is shown at the adhesion. The cross correlation is very small and it can be attributed to the bleed trough effect.

DISCUSSION

Techniques developed to achieve super-resolution like photoactivated localization microscopy and stochastic optical reconstruction microscopy are based on intensity fluctuations of single molecules induced by external means (1,14). The RICS method is also based on fluctuations, but they are number fluctuations due to the presence of a molecule or complex in the excitation volume. In the super-resolution techniques, the induced fluctuation must be maintained long enough to determine the position of the particle. During the fluctuation (or sampling time) the particle cannot move. Thus, there is a trade-off between the duration of the fluctuation and the spatial resolution. In the RICS method intensity fluctuations are measured on a very fast timescale. The

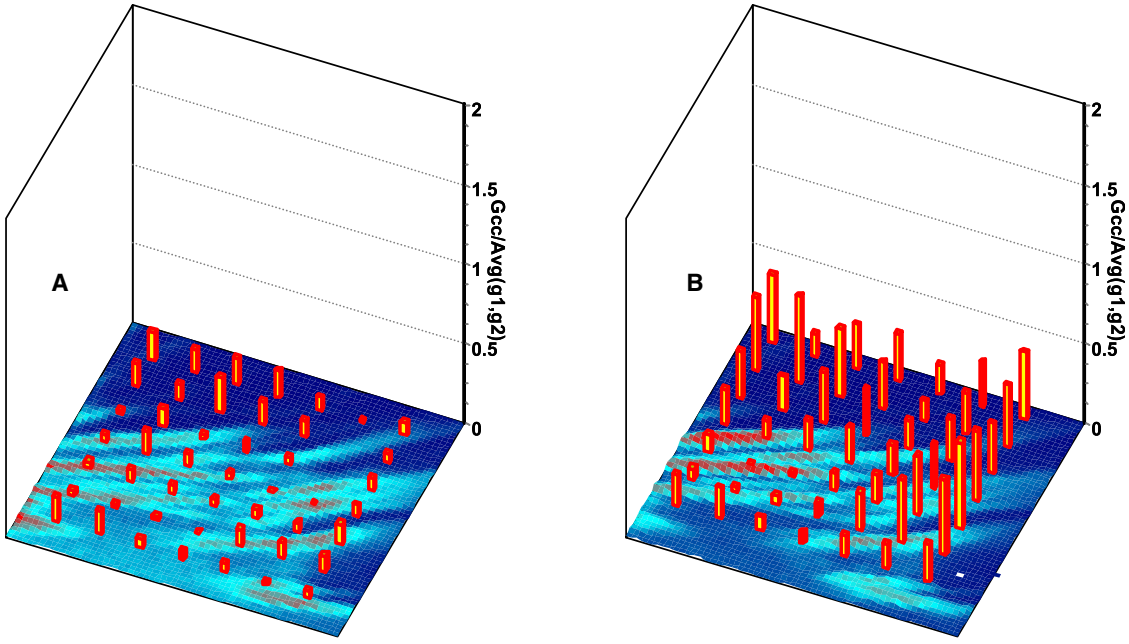

FIGURE 4 Map of the ccRICS signal normalized to the average of the autocorrelation function in both channels. (*A*) Obtained using a moving average length of 10 frames. (*B*) Obtained using a moving average of 40 frames. The upper part of the cell corresponds to the region where adhesions are disassembling.

change in position of the particle during the sampling time is used to determine its physical properties such as mobility, composition and number. However, this information content comes at the expense of spatial resolution. The RICS method is intrinsically 3D and relatively low resolution. When compared with the single molecule imaging methods, the

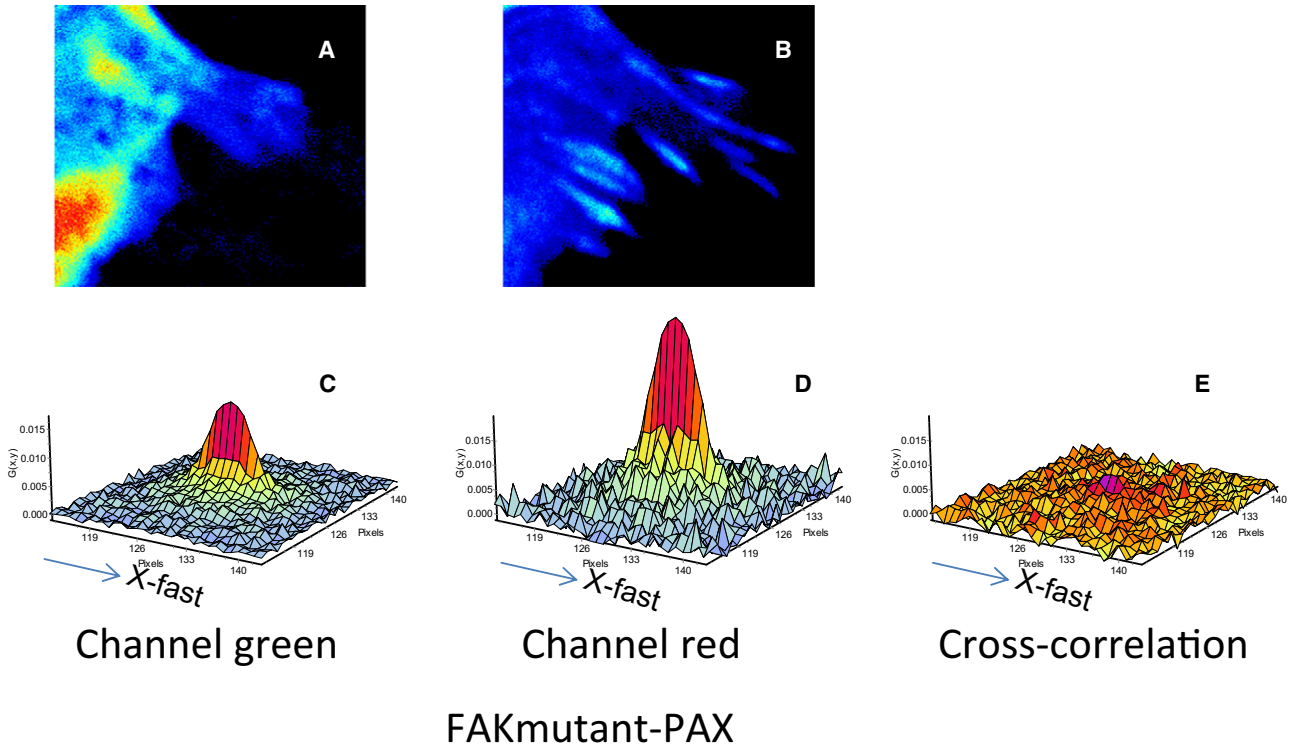

FIGURE 5 Cell expressing FAKmut-EGFP and PAX-mCherry. The size of the image is 12.5 μm by 12.5 μm. (*A*) The FAK mutant is not binding to Paxillin and is not concentrated at the adhesion. (*B*) Paxillin binds to the adhesion. (*C* and *D*) RICS autocorrelation of the green and red channels, respectively after immobile subtraction using a moving average length of 40. (*E*) The ccRICS is virtually nil except for the bleed through effect.

fluctuation analysis can better characterize the nature of the particle and the physical origin of the intensity fluctuation. Although we use the temporal part of the intensity fluctuations to determine mobility and complex composition in this study, it is possible to use the amplitude of the fluctuation to determine the stoichiometry of the fluctuating particles adding further information that can be extracted from analysis of fluctuations.

We have applied the RICS method to study the dynamics of cell-substrate adhesion complexes. These adhesions can be highly dynamic, and form and disassemble in minutes or less. Over 100 proteins (15) associate with adhesions, most of which are thought to reside in multimolecular complexes, based on immunoprecipitation and/or colocalization studies. A critical biological question, therefore, is which proteins do in fact reside in such a discrete structural complex and in what ratio, and when and where do these interactions occur. In this context, we have asked whether adhesions form or disassemble by the addition or subtraction of preassembled complexes.

We studied two pairs of proteins that are known to interact by coimmunoprecipitation and colocalize in adhesions (16). Surprisingly, we found that neither of the protein pairs are interacting in the cytoplasm, suggesting that adhesions do not form from addition of freely diffusing, preformed cytoplasmic complexes. However, we do see complexes at disassembling adhesions. In these cells, the cytoplasmic concentration of these molecules is low—probably too low to support their spontaneous association by mass action. From this, a picture emerges in which the assembling adhesion itself serves as a scaffold for the assembly of the protein complexes. In contrast, the large adhesions that we have studied disassemble by the release of complexes. In disassembling edges of adhesions, we see FAK-pax and vinculin-pax complexes exchanging from/leaving adhesions, and their subsequent diffusion away from the adhesion. However, the complexes are short lived and are not seen far from the adhesion, suggesting that they disassemble by mass action once out of the adhesion. As a consequence of the monomer addition (assembly) and large aggregate subtraction (disassembly), the adhesion appears to move or slide gradually. Thus, this sliding movement seems to be due to a treadmilling rather than the macroscopic movement (sliding) of the entire adhesion (17,18). This distinction was shown elegantly in a recent study of the apparent movement of adhesions using the photoactivated localization microscopy technique (19). It is important, therefore, to distinguish localized molecular events from macroscopic intensity changes, which are the sum of many events. These observations were made possible by large dynamic range of ccRICS, which simultaneously measures the diffusion, composition, and exchange of complexes.

The ccRICS methodology provides rich information about protein interactions. It can distinguish between different phenomena such as diffusion of protein aggregates and binding events involving protein complexes. We were able to separate these events on the basis of timescale and the different RICS functions that these two events provide. To illustrate the different signatures of diffusion and binding, we carried out simulations of particles diffusing in a plane (Fig. 1). We found that binding and diffusion occur at two different timescales, and we were able to separately identify the two processes and to quantify the timescale and the level of cross correlation on the basis of the different shape and amplitude of the ccRICS function (elongated versus round). The spatial map of the ccRICS amplitude provides further information about the cell compartments (adhesion regions) where some interactions occur preferentially. The spatial information shows that there is a gradient of protein complexes that are emanating from the disassembling adhesions. The existence of this gradient shows that we cannot calculate the equilibrium constant of the complex formation from the relative population of the free diffusing molecules and complexes. The formation of the complex is catalyzed by the scaffold at the adhesion and not by the mutual affinity of the individual proteins. It is the specific spatial information provided by ccRICS that allow us to establish the nature of the interactions and to properly interpret the origin of the complex formation.

The model of the disassembling of focal adhesions arising from the ccRICS implies that relatively large protein aggregates detach from the adhesions and then rapidly crumble in small parts that are still visible at a short distance from the disassembling adhesions. One important question is the stoichiometry of these aggregates immediately after they detach from the adhesion, because they could show the size and composition of the complexes at the adhesions. From the ccRICS studies we can only infer that the aggregates contain multiple proteins. In a previous study we determined that there are ~8–10 copies of paxillin in these disassembling aggregates (18). From the existence of a cross correlated signal and from the ratio of the $G(0,0)$ for the cross correlation to the $G(0,0)$ of the autocorrelation we infer that both vinculin and FAK are also present in multiple copies. A more quantitative analysis will require the statistical analysis of the fluctuation amplitudes and their correlations in the two channels.

In conclusion, RICS and ccRICS carry the information about the existence, composition, and dynamics of molecular complexes. Colocalization methods are insufficient to establish molecular aggregation, and coimmunoprecipitation does not establish that a particular interaction occurs in cells. By exploiting correlated molecular fluctuations available in single, dual channel confocal images, we can unequivocally establish the formation of molecular complexes in live cells and map their location. In addition, we can also separate binding from diffusion and eliminate problems due to bleaching, immobile components, and movement of edges and other structures. In contrast to previous image based two-color correlation measurements, which have two photon

excitation or other sophisticated hardware, two-color ccRICS can be done on commercial scanning confocal microscopes, and therefore is accessible to many more researchers in the health and biomedical sciences.

SUPPORTING MATERIAL

Two movies are available at http://www.biophysj.org/biophysj/supplemental/S0006-3495(08)00079-9.

We thank Jenny Sasaki for cultivating and transfecting the MEF cells.

This work was supported in part by U54 GM064346 Cell Migration Consortium (M.D., A.H., E.G.) National Institutes of Health grants P41-RRO3155 and P50-GM076516 (E.G.), the Natural Sciences and Engineering Research Council of Canada, and the Canadian Institutes of Health Research (P.W.W.).

REFERENCES

1. Betzig, E., G. H. Patterson, R. Sougrat, O. W. Lindwasser, S. Olenych, et al. 2006. Imaging intracellular fluorescent proteins at nanometer resolution. *Science*. 313:1642–1645.
2. Gustafsson, M. G. 2008. Super-resolution light microscopy goes live. *Nat. Methods*. 5:385–387.
3. Weiss, S. 2000. Shattering the diffraction limit of light: a revolution in fluorescence microscopy? *Proc. Natl. Acad. Sci. USA*. 97:8747–8749.
4. Willig, K. I., S. O. Rizzoli, V. Westphal, R. Jahn, and S. W. Hell. 2006. STED microscopy reveals that synaptotagmin remains clustered after synaptic vesicle exocytosis. *Nature*. 440:935–939.
5. Jares-Erijman, E. A., and T. M. Jovin. 2006. Imaging molecular interactions in living cells by FRET microscopy. *Curr. Opin. Chem. Biol.* 10:409–416.
6. Liebler, D. C. 2002. Proteomic approaches to characterize protein modifications: new tools to study the effects of environmental exposures. *Environ. Health Perspect.* 110 (*Suppl 1*):3–9.
7. Bacia, K., S. A. Kim, and P. Schwille. 2006. Fluorescence cross-correlation spectroscopy in living cells. *Nat. Methods*. 3:83–89.
8. Digman, M. A., C. M. Brown, P. Sengupta, P. W. Wiseman, A. R. Horwitz, et al. 2005. Measuring fast dynamics in solutions and cells with a laser scanning microscope. *Biophys. J.* 89:1317–1327.
9. Digman, M. A., P. Sengupta, P. W. Wiseman, C. M. Brown, A. R. Horwitz, et al. 2005. Fluctuation correlation spectroscopy with a laser-scanning microscope: exploiting the hidden time structure. *Biophys. J.* 88: L33–L36.
10. Brown, C. M., R. B. Dalal, B. Hebert, M. A. Digman, A. R. Horwitz, et al. 2008. Raster image correlation spectroscopy (RICS) for measuring fast protein dynamics and concentrations with a commercial laser scanning confocal microscope. *J. Microsc.* 229:78–91.
11. Wiseman, P. W., J. A. Squier, M. H. Ellisman, and K. R. Wilson. 2000. Two-photon image correlation spectroscopy and image cross-correlation spectroscopy. *J. Microsc.* 200:14–25.
12. Das, R., S. Hammond, D. Holowka, and B. Baird. 2008. Real-time cross-correlation image analysis of early events in IgE receptor signaling. *Biophys. J.* 94:4996–5008.
13. Petersen, N. O., and E. L. Elson. 1986. Measurements of diffusion and chemical kinetics by fluorescence photobleaching recovery and fluorescence correlation spectroscopy. *Methods Enzymol.* 130:454–484.
14. Rust, M. J., M. Bates, and X. Zhuang. 2006. Sub-diffraction-limit imaging by stochastic optical reconstruction microscopy (STORM). *Nat. Methods*. 3:793–795.
15. Zaidel-Bar, R., S. Itzkovitz, A. Ma'ayan, R. Iyengar, and B. Geiger. 2007. Functional atlas of the integrin adhesome. *Nat. Cell Biol.* 9:858–867.
16. Choi, C., M. Vicente-Manzanares, J. Zareno, L. A. Whitmore, A. Mogilner, et al. 2008. Actin and alpha-actinin orchestrate the assembly and maturation of nascent adhesions in a myosin II motor-independent manner. *Nat. Cell Biol.* 10:1039-1050.
17. Wehrle-Haller, B., and B. A. Imhof. 2003. Actin, microtubules and focal adhesion dynamics during cell migration. *Int. J. Biochem. Cell Biol.* 35:39–50.
18. Digman, M. A., C. M. Brown, A. R. Horwitz, W. W. Mantulin, and E. Gratton. 2008. Paxillin dynamics measured during adhesion assembly and disassembly by correlation spectroscopy. *Biophys. J.* 94:2819–2831.
19. Shroff, H., C. G. Galbraith, J. A. Galbraith, and E. Betzig. 2008. Live-cell photoactivated localization microscopy of nanoscale adhesion dynamics. *Nat. Methods*. 5:417–423.